Geomorphology 303 (2018) 271–283

Contents lists available at ScienceDirect

Geomorphology

journal homepage: www.elsevier.com/locate/geomorph

Late Pliocene establishment of exorheic drainage in the northeastern Tibetan Plateau as evidenced by the Wuquan Formation in the Lanzhou Basin

Benhong Guo [a], Shanpin Liu [a], Tingjiang Peng [a], Zhenhua Ma [a], Zhantao Feng [a], Meng Li [a], Xiaomiao Li [a], Jijun Li [a,b,*], Chunhui Song [c], Zhijun Zhao [b], Baotian Pan [a], Daniel F. Stockli [d], Junsheng Nie [a]

[a] Key Laboratory of Western China's Environmental Systems (Ministry of Education), College of Earth and Environmental Sciences, Lanzhou University, Lanzhou 730000, China
[b] College of Geography Science and Key Laboratory of Virtual Geographic Environment (Ministry of Education), Nanjing Normal University, Nanjing 210023, China
[c] School of Earth Sciences and Key Laboratory of Western China's Mineral Resources (Gansu Province), Lanzhou University, Lanzhou 730000, China
[d] Department of Geological Sciences, Jackson School of Geosciences, University of Texas at Austin, Austin, TX, USA

ARTICLE INFO

Article history:
Received 21 August 2017
Received in revised form 3 December 2017
Accepted 3 December 2017
Available online 8 December 2017

Keywords:
Fluvial system
Tibetan Plateau
Provenance
Late Pliocene

ABSTRACT

The fluvial archives in the upper-reach Yellow River basins provide important information about drainage history of the northeastern Tibetan Plateau (TP) associated with geomorphologic evolution and climate change. However, the Pliocene fluvial strata within this region have not been studied in detail, hence limiting the understanding of the late Cenozoic development of regional fluvial systems. In this paper, we present the results of a study of the geochronology, sedimentology, and provenance of the fluvial sequence of the Wuquan Formation in the Lanzhou Basin in the northeastern TP. Magnetostratigraphic and cosmogenic nuclide burial ages indicate that the Wuquan Formation was deposited during 3.6–2.2 Ma. Furthermore, sedimentary facies, gravel composition, paleocurrent data, and detrital zircon U—Pb age spectra reveal that the fluvial sequence resembles the terraces of the Yellow River in terms of source area, flow direction, and depositional environment. Our results indicate that a paleo-drainage system flowing out of the northeastern TP was established by ca. 3.6 Ma and that the upstream parts of the Yellow River must have developed subsequently from this paleo-drainage system. The late Pliocene drainage system fits well with the dramatic uplift of the northeastern TP, an intensified Asian summer monsoon, and global increase in erosion rates, which may reflect interactions between geomorphic evolution, tectonic deformation, and climate change.

1. Introduction

Cenozoic uplift of the Tibetan Plateau (TP) has been thought to have significantly influenced regional erosion and global climate change, which might also have affected topographic evolution of the TP (Molnar and England, 1990; Raymo and Ruddiman, 1992; Zhang et al., 2001; Whipple, 2009). In response to the initiation of uplift, the fluvial system would have been subjected to reorganization and thus provides a critical record of topographic evolution associated with past tectonics and/or climate change (Clark et al., 2004; Clift and Blusztajn, 2005; Zheng et al., 2013; Wang et al., 2014; Nie et al., 2015).

Originated from the northeastern TP, the Yellow River is the second largest river in China (Fig. 1) and has an important impact on regional landscape development and sediment transportation. The Yellow River is deeply incised into a series of intermontane basins and tectonic ranges in its upper and middle reaches, forming multistage terraces. Based on the chronological framework of these terraces, the Yellow River is indicated to have been formed since the middle Pleistocene or later (~0.1 Ma) as a result of tectonic uplift of the northeastern TP (Li et al., 1996, 1997; Pan et al., 1996, 2009; Harkins et al., 2007; Hu et al., 2016, 2017; B.F. Li et al., 2017) or by the effect of climate change (Craddock et al., 2010; Perrineau et al., 2011; Kong et al., 2014). However, different lines of sedimentary and tectonic evidence have demonstrated that the major uplift of the northeastern TP and significant climate change commenced in the late Miocene and was intensified in the late Pliocene (Meyer et al., 1998; An et al., 2001; Zachos et al., 2001; Zhang et al., 2009; Fu et al., 2013; Craddock et al., 2014; Lease, 2014; Li et al., 2014; J.J. Li et al., 2017; Nie et al., 2017), which is substantially earlier than the uppermost terraces of the Yellow River. How regional topography evolved in response to late Miocene-Pliocene mountain building and climate change, followed by the formation of the Yellow River, are issues that remain poorly understood, mainly because of the absence of study of paleo-drainage in the northeastern TP.

The Lanzhou Basin situated on the margin of the northeastern TP and connecting upland areas upstream with lowlands downstream (Fig. 1)

* Corresponding author at: Key Laboratory of Western China's Environmental Systems (Ministry of Education), College of Earth and Environmental Sciences, Lanzhou University, Lanzhou 730000, China.
E-mail address: lijj@lzu.edu.cn (J. Li).

https://doi.org/10.1016/j.geomorph.2017.12.009
0169-555X/

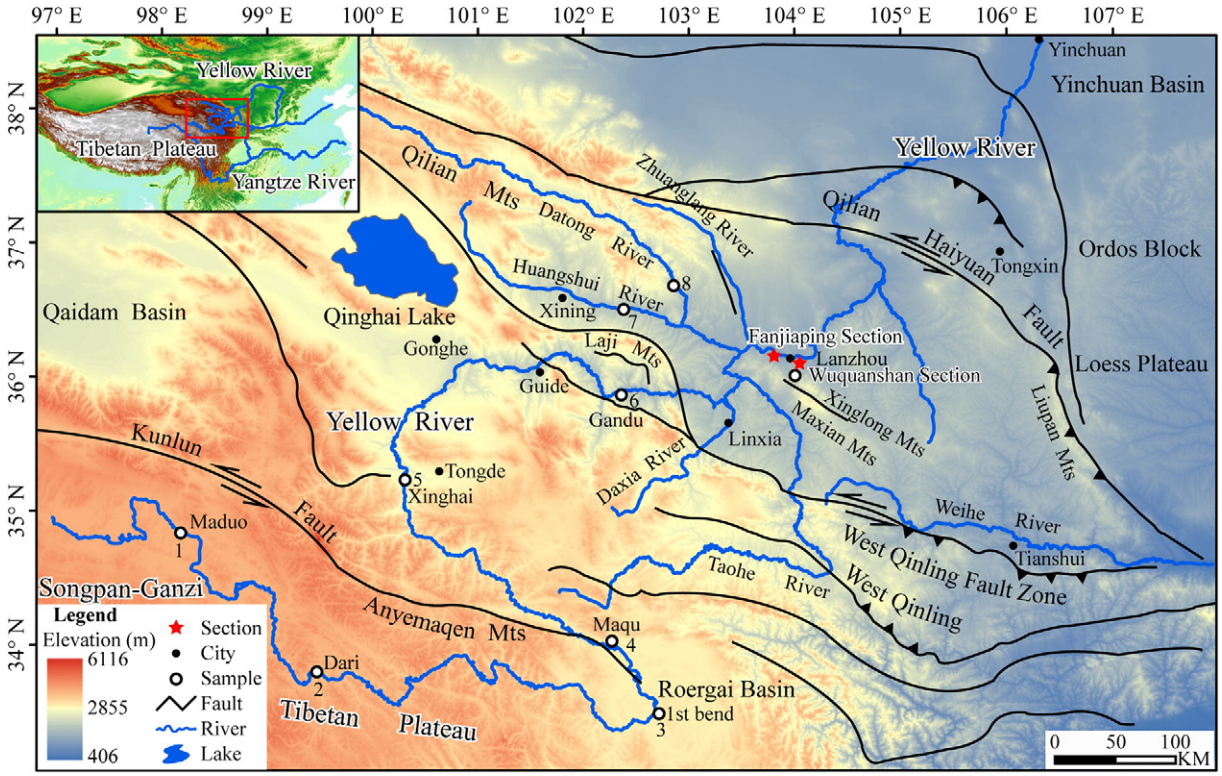

Fig. 1. Geographic setting of the Fanjiaping and Wuquanshan sections. DEM maps show the location of the Lanzhou Basin and surrounding mountains and their major tectonic and geomorphologic features. Inset map shows the location of the study area in north China. ArcGIS10.2 was used to create the base map. The SRTMDEMUTM 90-m data were obtained from http://www.gscloud.cn/.

is well-suited to testing whether paleo-rivers ran through the plateau margin. Specifically, the Lanzhou Basin contains a unique Pliocene to early Pleistocene fluvial archive in the form of the Wuquan Formation (Gu and Zhang, 1987; Wu et al., 1988), although its precise age, lithology, and provenance have not been studied in detail. This paper presents new data on paleomagnetic chronology, cosmogenic nuclide burial ages, detrital zircon U—Pb ages, and conglomerate analyses to illuminate the nature of the Wuquan Formation, as well as its implications for understanding long-term drainage history and geomorphic evolution of the northeastern TP, coupled with tectonic deformation and climate change.

2. Regional geological and geomorphic setting

The northeastern TP is tectonically bounded by the sinistral strike-slip Kunlun Fault to the south and the Qilian-Haiyuan faults to the north (Fig. 1). It consists of a series of NWW-trending high tectonic ranges (ca. 4000–5000 m in elevation), e.g., the Anyemaqen Mountains, the Eastern Kunlun Mountains, the West Qinling Mountains, and the Qilian Mountains. These ranges confine many sedimentary basins that contain hundreds to thousands of meters thickness of Cenozoic terrigenous sediments (Lease, 2014; Li et al., 2014; Fig. 1). The northeastern TP lies at the junction of the areas impacted by the East Asian monsoon, the northern arid climate, and the climate of the Tibetan highlands (Li et al., 2014; Zhang et al., 2016). In northeastern TP, the modern Yellow River flows from the Anyemaqen Mountains at ~3300 m elevation, descends through a series of basins and ranges, enters the Lanzhou Basin at ~1500 m elevation, and then turns northeastward at ~1000 m elevation (Fig. 1).

The late Cenozoic Lanzhou Basin is extruded east-west and stretched from south to north, being regulated by the Maxian-Xinglong Fault to the south and the Zhuanglang Fault to the west (Yuan, 2007; Yuan et al., 2008; Figs. 1 and 2). It belongs to the Qilian orogenic belt. The bounding ranges of the basin are the Qilian Mountains, the Maxian-Xinglong Mountains, and the Laji Mountains (Fig. 1), which consist largely of Precambrian and lower Paleozoic metamorphic rocks, early Paleozoic plutons, and Lower Cretaceous sedimentary rocks (Zhai and Cai, 1984; Gehrels et al., 2003; Tung et al., 2016). The geological setting contrasts significantly with the plateau ranges of the West Qinling and Songpan-Ganzi terranes, which are mainly composed of Triassic submarine fan deposits and Permo-Triassic plutons (Weislogel et al., 2010). Moreover, the Lanzhou Basin is filled with massive alluvial-lacustrine red strata dominated by successive mudstones, limestones, and gypsum intercalated with limited braided river and fan-delta sandstone layers with a total thickness of 1000–2000 m. The red strata are of Eocene to late Miocene age, based on magnetostratigraphy constrained by biostratigraphy (Yue et al., 2000; Y.P. Zhang et al., 2014; Ao et al., 2016; Wang et al., 2016). Following the termination of basin infilling, the Wuquan Formation and pediment surface were formed in the late Pliocene or early Quaternary (Gu and Zhang, 1987; J.J. Li et al., 2017). The Yellow River continued to cut downward and to develop a series of terraces (Li et al., 1996, 1997). This sedimentary sequence is overlain by a Quaternary loess-paleosol sequence with a typical thickness of 400 m (Burbank and Li, 1985; Li et al., 1999; Zhang et al., 2016).

The Wuquan conglomerate, originally named as the Wuquanshan System by Young and Bien (1937), unconformably overlies the Eocene-Miocene red beds. The two main outcrops within the Lanzhou Basin are the Fanjiaping and Wuquanshan sections. The Fanjiaping section (36°04′55.9″ N, 103°40′07.8″ E; Figs. 1 and 2) is on the southern bank of the Yellow River, in the depocenter of the Qilihe depression zones, which are dominated by the Leitanhe, Shengouqiao, Xijincun, and Jinchengguan faults. The Wuquanshan section (36°01′50″ N, 103°49′48″ E; Figs. 1 and 2), which lies on the hanging wall of the Leitanhe thrust fault (Yuan et al., 2008), is composed mainly

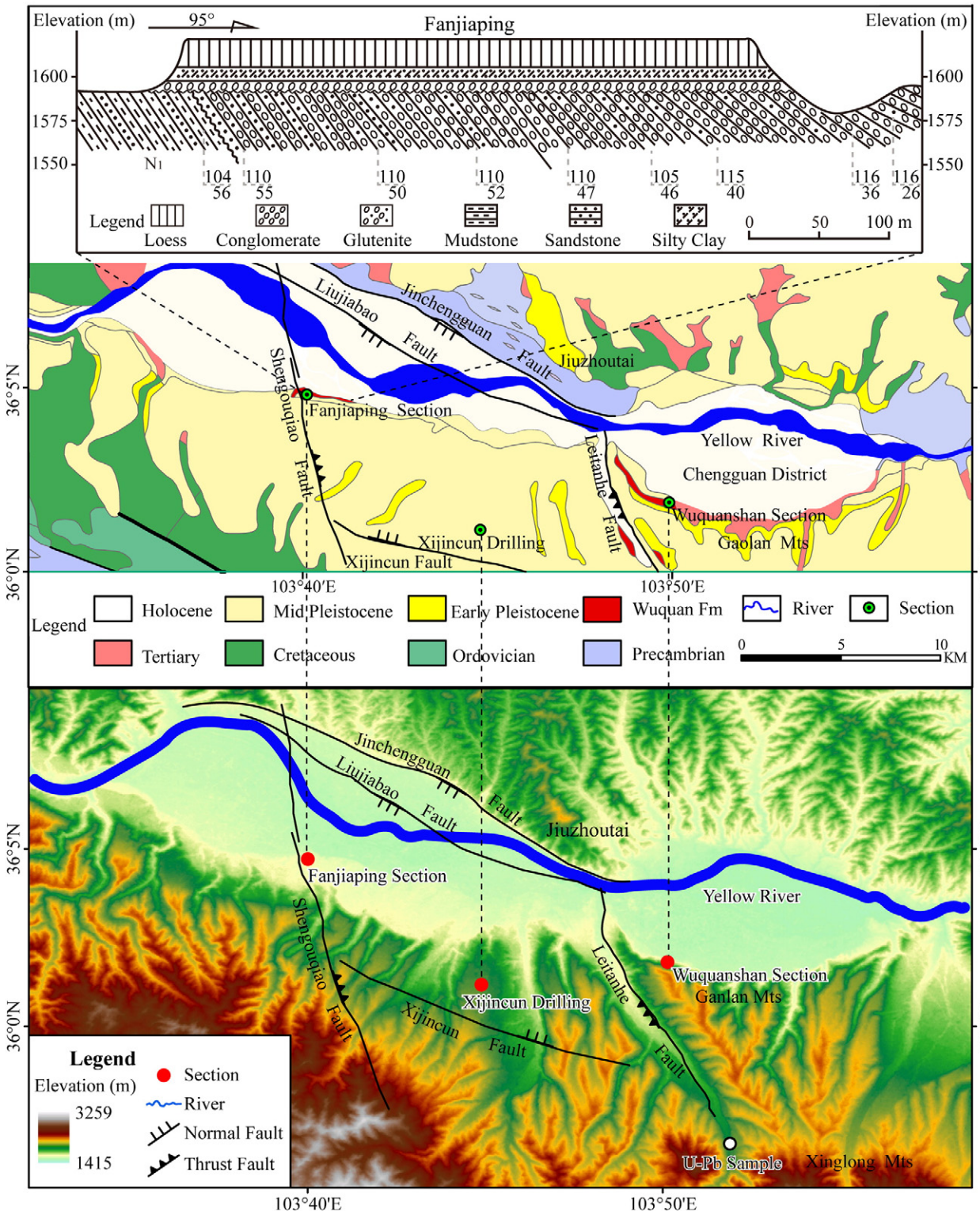

Fig. 2. Geological and geomorphological context of the Fanjiaping and Wuquanshan sections and the Xijincun drill site in the Lanzhou Basin. Geological map of the Lanzhou Basin modified from Gansu BGMR (1988). ArcGIS10.2 was used to create the base map. The SRTMDEMUTM 30-m data were obtained from http://www.gscloud.cn/.

of grey, well-rounded, well-sorted graded beds of pebble-cobble conglomerates, intercalated with channelized or lenticular sandstones (Fig. 3). The Fanjiaping and Wuquanshan sections expose sediments that are respectively 440 and 100 m thick with steep dip angles slightly less than those of the underlying beds (Fig. 2). The Wuquan Formation is mainly covered by Quaternary loess and/or Yellow River terraces. Previous research has determined loess ages of 2.2 Ma in the Xijingcun drill core and 1.6 Ma in the Wuquanshan section (Li et al., 1999; Zhang et al., 2016).

3. Materials and methods

Systematic chronostratigraphic, lithologic, and provenance studies were performed to assess the age of initial formation of the paleo-river

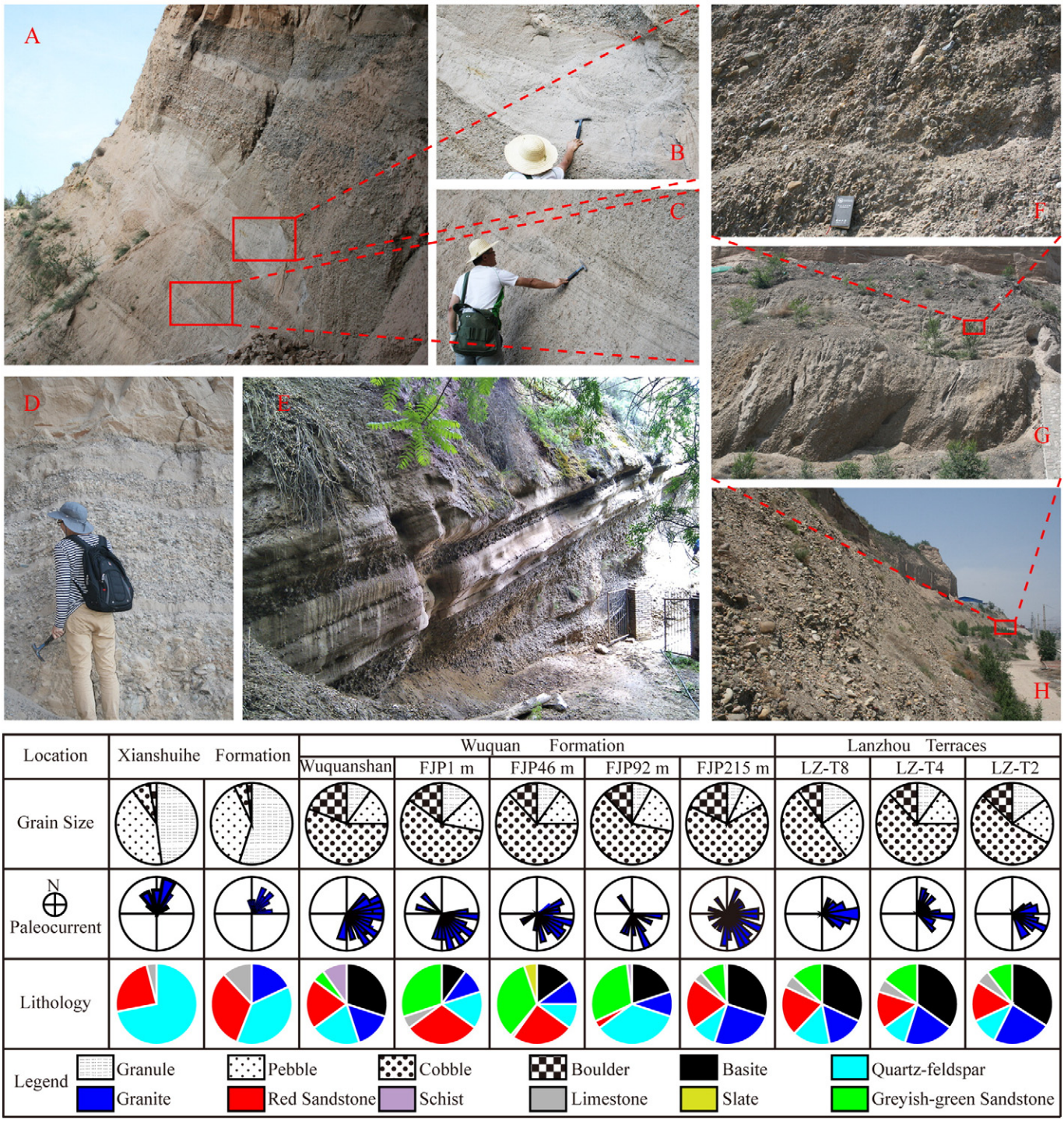

Fig. 3. Sedimentary structures of the Wuquanshan and Fanjiaping sections. Photographs show the main sedimentary characteristics of the Wuquanshan (A, B, C, D, E) and Fanjiaping (F, G, H) sections. The figure illustrates changes in lithology, paleocurrent direction, and grain size in the Xianshuihe Formation, Wuquan Formation, and Lanzhou terraces.

system. To establish a more accurate chronology for the Wuquan Formation, the Fanjiaping and Wuquanshan sections were dated by magnetostratigraphy and cosmogenic radionuclides (^{10}Be and ^{26}Al) respectively. Studies of lithology, including sedimentary structures and textures, and quantitative measurements of gravel size, composition, and fabric, together with rock magnetic characterization, were conducted to reconstruct the ancient depositional environments and paleocurrent directions of the Wuquan Formation and to characterize the changes from red beds to terraces. Detrital zircon U—Pb dating was used to trace potential source regions and any change in provenance from the Tertiary strata to the terraces. Details of the techniques used are described below.

3.1. Rock magnetic measurements

To characterize the magnetic mineralogy, a total of 12 representative samples from different sandy lenses in the Fanjiaping section were collected for measurements of low-field temperature-dependent magnetic susceptibility (*k*-T curves) and magnetic hysteresis. The *k*-T curves were obtained using an MFK-1-FA Kappabridge magnetic susceptibility

meter equipped with a CS-4 temperature control apparatus from room temperature to 700 °C and back to room temperature. A heating/cooling rate of 11°/min was used and the measurements were made in an argon atmosphere to prevent oxidation. The measurements were made at the Institute of Tibetan Plateau Research, Chinese Academy of Sciences (CAS), Beijing. Hysteresis loops in a maximum field of 1 T were obtained using a Vibrating Sample Magnetometer at the Key Laboratory for Magnetism and Magnetic Materials of the Ministry of Education, Lanzhou University. The loops were corrected for paramagnetic contributions (Fig. 4).

3.2. Paleomagnetic measurements

For the Fanjiaping section, paleomagnetic sampling locations were selected where possible in sandy mudstone, siltstone, and fine-grained sandstone layers, and the oriented samples were fixed with silica adhesive. The sampling interval was 2–20 m, depending on the occurrence of sand lenses within the conglomerate layers. A total of 114 block samples were obtained. In the laboratory, the oriented blocks of roughly 10 × 10 × 8 cm were cut into cubic specimens of dimensions 2 × 2 × 2 cm to produce three parallel sets of samples enabling cross-checking. Previous studies indicated that a single set of paleomagnetic samples treated using thermal demagnetization can recover most of the polarity intervals within the studied sequence (Zheng et al., 2000; Fang et al., 2003; Craddock et al., 2010). All samples were stored, demagnetized, and measured within a magnetically shielded space where the internal geomagnetic field was <200 nT. All samples were subjected to thermal demagnetization with 18 steps at 20–50 °C increments to a maximum temperature of 680 °C using an MMTD80 thermal demagnetizer. The remanent magnetizations were measured using a 2G Enterprise 760 Cryogenic Superconducting Magnetometer. Ninety percent of the paleomagnetic samples were measured at the Paleomagnetic and Rock Magnetic Laboratory of the Key Laboratory of Western China's Environment (Ministry of Education) at Lanzhou University and the remainder were measured at the Institute of Tibetan Plateau Research, Chinese Academy of Sciences (CAS), Beijing. The direction of the characteristic remnant magnetization was determined by principal component analysis (Kirschvink, 1980).

3.3. $^{26}Al/^{10}Be$ burial age measurements

For the Wuquanshan section, two in situ samples of coarse fluvial sand were collected for analysis of cosmogenic ^{26}Al and ^{10}Be inventories in quartz grains. Sample WQA (32-m depth) was collected from a coarse sand layer at the base of a recent 30-m-deep landslide cave. Sample WQB (25-m depth) was collected from a quartz-rich sand layer within a 5-m-deep artificial hole ~20 m below the top of the excavated wall. The sampled locations were unweathered and clearly exhibited primary sedimentary structures. Quartz grains were extracted in the Mineral Separation Laboratory of Purdue University, IN, USA, and ^{10}Be and ^{26}Al concentrations were measured using accelerator mass spectrometry and an inductively-coupled plasma-optical emission spectrometer at the Purdue University Rare Isotope Measurement Laboratory. Sample treatment, nuclide measurements, and age calculations were conducted using conventional procedures (Nishiizumi et al., 2007; Hu et al., 2011; Zhao et al., 2017).

3.4. Detrital zircon U—Pb measurements

Ten sand samples were collected from the two sections, from the eighth terrace (Li et al., 1996), the modern Yellow River and its tributaries (Leitan River and Datong River) (Figs. 1, 2, 7 and 8). To minimize the potential bias of the zircon age distribution in a poorly mixed depositional environment (DeGraaff-Surpless et al., 2003), samples of ~5 kg were obtained by mixing material from several locations within a same layer or catchment respectively. Detrital zircon grains were separated and concentrated using standard heavy liquid techniques. >100 grains were then randomly selected and fixed with epoxy resin using double-sided tape to ensure that the main crystal plane of the grains faced upward. The U—Pb isotopes were measured using laser ablation high-resolution inductively-coupled plasma mass spectrometry (LA-ICP-MS) with an Element2 instrument

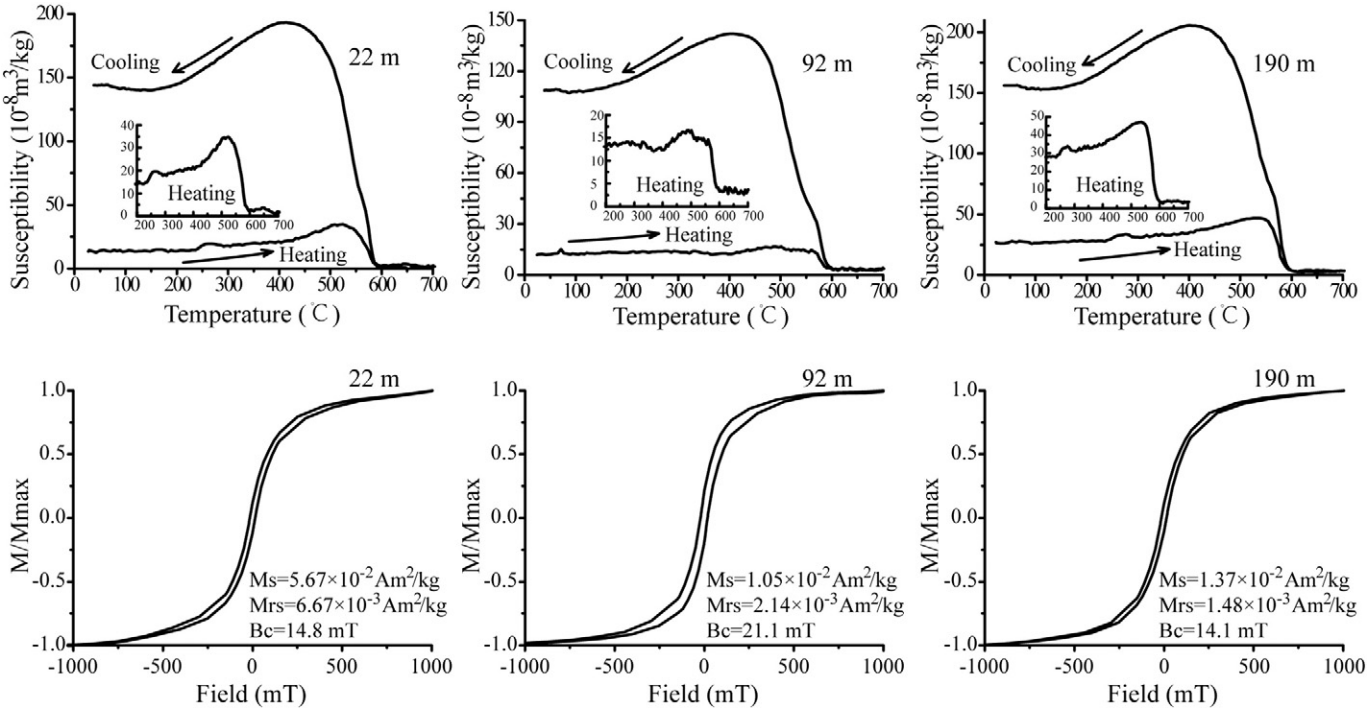

Fig. 4. The *k*-T curves (upper) and hysteresis loops (lower) for representative samples from the Fanjiaping section. The hysteresis loops are corrected for the paramagnetic contributions.

at the Thermochronometry Laboratory at the University of Texas at Austin and the Key Laboratory of Western China's Mineral Resources (Gansu Province), Lanzhou University. Established methods (Kong et al., 2014; Liu et al., 2015) were used to perform data reduction and correction. The $^{206}Pb/^{238}U$ ages were accepted for the ages younger than 1 Ga, while $^{207}Pb/^{206}Pb$ ages were accepted for the ages older than 1 Ga. Following standard data filters (Lease et al., 2007), zircon ages with ≥30% discordance or ≥10% reverse discordance were excluded. The resulting age distributions were plotted as probability density functions and histograms (Fig. 8).

4. Results

4.1. Lithology of the Wuquan Formation

The lower part of the Wuquan Formation (0–40 m in the Wuquanshan section, 0–195 m in the Fanjiaping section) is composed of 6–11 cycles of alternating conglomerate and sand layers (Fig. 7). The sequences exhibit normal graded bedding and cross-bedding structures, which strongly suggest a channelized depositional environment (Wu et al., 1988; Fig. 3). Most of the conglomerate layers are well sorted, with 60–70% cobbles, 15–20% pebbles, and <30% granules (Fig. 3). Rounded and subrounded gravels account for >80% of the total. Imbrication fabrics are widespread in the conglomerate strata, exhibiting an eastward or southeastward orientation (Fig. 3). The gravel composition is complex, with the majority of the clasts consisting of metamorphic greyish-green sandstones, red sandstones, basites, granites, quartz, and feldspars (Fig. 3). All of these characteristics of the lower Wuquan Formation resemble those of the Yellow River terraces but are significantly different from those of the underlying red beds (Fig. 3).

In contrast, the upper part of the Wuquan Formation (40–100 m of the Wuquanshan section, 195–443 m of the Fanjiaping section) consists of less sand and more boulder conglomerates, indicating a more rapid deposition rate (Wu et al., 1988). Furthermore, the proportion of angular clasts is greater in the Wuquanshan section, and the sedimentary structures are more disordered; however, the main flow direction and gravel composition are not significantly different from the lower part.

4.2. Rock magnetic properties

The *k*-T curves and hysteresis loops of typical samples from the Fanjiaping section are illustrated in Fig. 4. Each *k*-T heating curve exhibits an increasing trend with a peak at about 510 °C (Fig. 4), which is not present in the cooling curve. Thus, this latter feature is unlikely to be the Hopkinson peak and instead probably reflects the neoformation of magnetic minerals at that temperature (Deng et al., 2001). In addition, the heating curve exhibits a distinct decrease near 580 °C, corresponding to the Curie temperature of magnetite (Deng et al., 2005), while a gradual decrease of susceptibility at around 680 °C indicates the presence of hematite. Most of the hysteresis loops are not closed until at least ~500 mT, indicating the significant presence of imperfect antiferromagnetic minerals such as hematite or goethite (Deng et al., 2006). This finding is also supported by the inflections in the corresponding *k*-T curves at ~120 °C and ~650 °C. In addition, the waspwaisted loops (Fig. 4) clearly indicate the coexistence of magnetic minerals with different coercivities and/or magnetic grain sizes (Evans and Heller, 2003).

4.3. Paleomagnetic and cosmogenic nuclide burial dating

Paleomagnetic analyses were carried out to establish a magnetostratigraphy for the Fanjiaping section. After removal of a low temperature viscous component, the characteristic remnant magnetization (ChRM) was successfully isolated (Fig. 5). The demagnetization behavior indicates that magnetite is the dominant ChRM carrier, which is consistent with the rock magnetic results and with previous paleomagnetic studies of late Pliocene conglomerates in the intermountain basins surrounding the TP (Zheng et al., 2000; Fang et al., 2003; Craddock et al., 2010). In the orthogonal vector demagnetization plots the ChRM is represented by a unidirectional decay toward the origin from 250 to 680 °C (Fig. 5). Data from at least 4 (but typically 6–10) consecutive demagnetization steps above 250 °C were used to determine the ChRM direction, with a maximum angular deviation (MAD) of <15° (but typically 4–10°) for the respective line fits. From the 114 demagnetized levels, 89 (78%) yielded reliable ChRM components based on strict selection criteria. The virtual geomagnetic pole (VGP) latitudes calculated from the 89 ChRM directions were used to establish a magnetostratigraphy (Fig. 7).

All of the accepted tilt-corrected ChRM directions of the Fanjiaping section were used for a reversal test. As shown in Fig. 6A, the mean direction of the normal polarity sites ($D = 53.3°$, $I = 44.8°$, $\alpha95 = 6.5$, $k = 74$) is roughly antiparallel to the mean direction of the reversed-polarity sites ($D = 217.3°$, $I = -48.1°$, $\alpha95 = 10.5$, $k = 15$), indicating a positive reversal test (Tauxe, 1998). These findings confirm that the ChRM is the primary remanence (Tauxe, 1998). Furthermore, a jackknife analysis (Tauxe and Gallet, 1991) produced a jackknife parameter J of −0.2983 for the observed polarity zones, which falls within the range of 0 to −0.5 recommended by Tauxe and Gallet (1991) for a robust magnetostratigraphic data set. This result indicates that the sampling of this section has recovered >95% of the true number of polarity intervals (Fig. 6B). In addition, this combined site mean direction passes the McFadden (1990) fold test at the 95% confidence level and yields a maximum grouping at 90.1% unfolding (Fig. 6C), which indicates a positive fold test. The reversal test, jackknife analysis, and fold tests suggest that >95% of the true number of polarity intervals have been recovered by the field sampling (Figs. 6 and 7). Based on the foregoing, a total of three normal polarity zones (N1-N3) and two reversed polarity zones, R1 (198–177 m) and R2 (122–92.5 m), are present in the Fanjiaping section (Fig. 7).

The results of cosmogenic nuclide burial dating of the Wuquanshan section provide further constraints on the chronology of the Wuquan Formation. The two samples were buried to depths of more than ~10 m, and it is assumed that post-burial production of cosmogenic nuclides was negligible during the sedimentation process. The concentrations of cosmogenic nuclides (^{10}Be and ^{26}Al) and burial ages of the two samples are listed in Table 1. The measured ^{10}Be concentrations are 8.47×10^3 and 9.23×10^3 atoms/g of quartz, while ^{26}Al concentrations are 15.49×10^3 and 17.87×10^3 atoms/g. The $^{26}Al/^{10}Be$ ratios of the two samples are 1.94 ± 0.43 and 1.83 ± 0.46. To calculate the approximated burial ages for these samples, we need to estimate either pre-burial or post-burial erosion rates of the landforms. The correction and calculation method used was modified from other studies of the Yellow River and of conglomerate deposits (Granger and Muzikar, 2001; Hu et al., 2011; Zhao et al., 2017). After careful analysis, the cosmogenic ^{10}Be and ^{26}Al burial ages were calculated, and they indicate that the burial ages of the two samples (WQA and WQB) are $2.72 + 0.54/-0.46$ and $2.85 + 0.60/-0.52$ Ma respectively. The burial ages are consistent with the stratigraphic sequence of the Wuquan Formation.

4.4. Detrital zircon U—Pb ages

We used the density plotter (Vermeesch, 2012) to compile and plot zircon U—Pb age spectra as probability density functions (PDF), kernel density estimates (KDE), and histograms for the samples from the Wuquan Formation, the eighth terrace, and modern fluvial bars (Fig. 8A–G, J, K and L). For comparison, we also compiled a list of published detrital zircon age data from the underlying red strata of the Xianshuihe Formation (Wang et al., 2016; Fig. 8H), the late Pliocene Jishi Formation, and the Ganhegou Formation in the Linxia and Tongxin basins (Wang et al., 2013; Nie et al., 2015; Fig. 8O, P), Quaternary loess in the Chinese Loess Plateau (Pullen

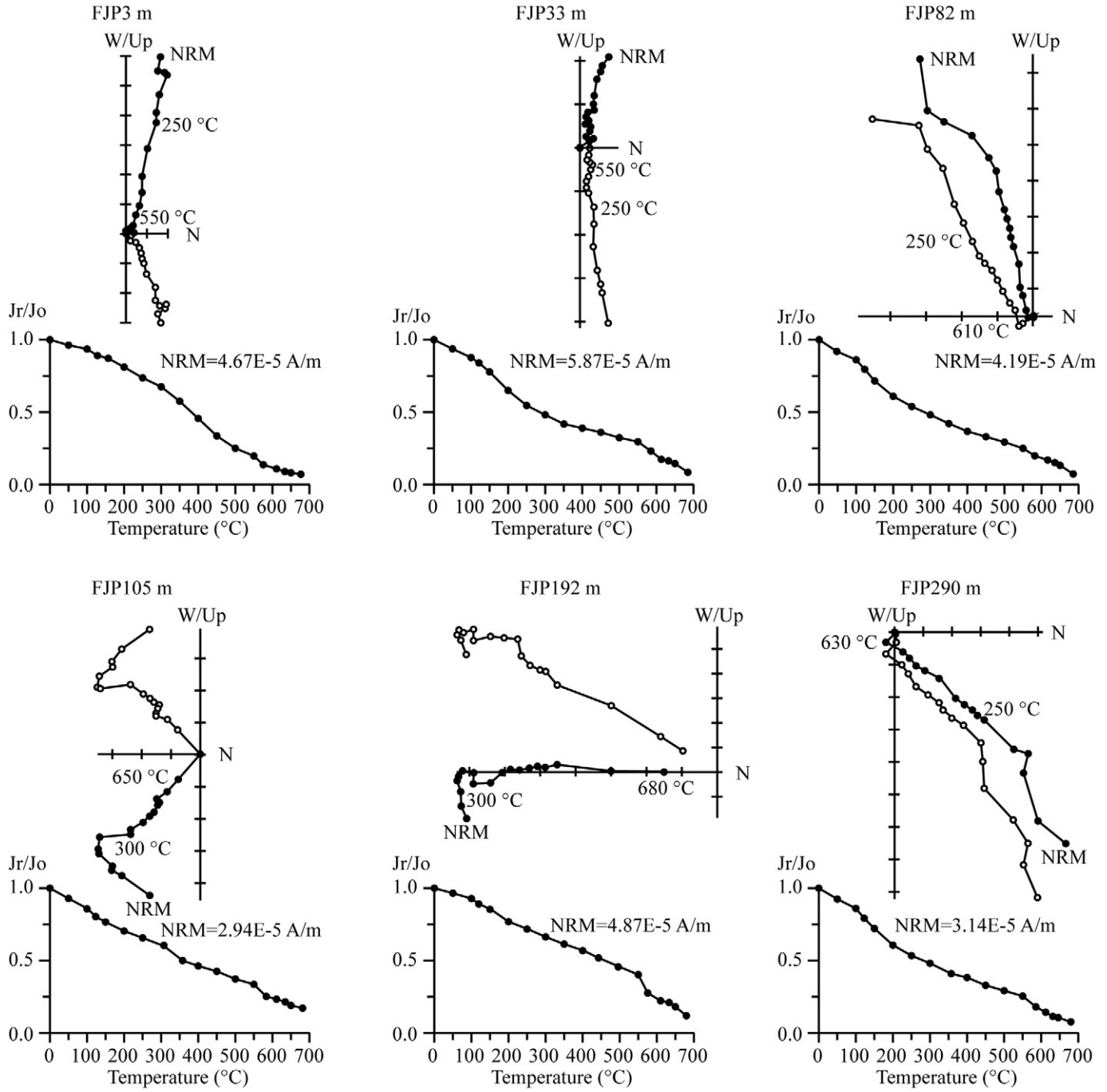

Fig. 5. Results of stepwise thermal demagnetization of representative samples from the Fanjiaping section. Directions are in situ. Solid and open circles represent vector endpoints projected onto horizontal and vertical planes respectively.

et al., 2011; Stevens et al., 2013; Fig. 8N), late Pleistocene terraces in Lanzhou Basin and modern bars in the upper reaches of the Yellow River (Nie et al., 2015; Fig. 8I and M).

As Fig. 8 clearly shows, the detrital zircon ages of the two samples from the Wuquan Formation are concentrated in two peaks with age ranges of 300–200 and 500–400 Ma, and with additional ages distributed within the ranges 1000–800, 2000–1600, and 2600–2400 Ma (Fig. 8B–G). The characteristic age spectra of the Wuquan Formation resemble the detrital zircon age spectra of the samples from the Yellow River terraces and modern channel bar within the Lanzhou Basin (Fig. 8A, L and M). In addition, they are broadly comparable to those of samples from modern bars along the upper reaches of the Yellow River, the Jishi Formation, the deposits from the Chinese Loess Plateau, and the Ganhegou Formation (Fig. 8I, N–P). In contrast, the age spectrum of the Xianshuihe Formation clearly lacks the peak corresponding to 500–400 Ma (Fig. 8H), while the samples from the Huangshui River and Datong River lack ages within the range 300–200 Ma (Fig. 8J). Moreover, in the Fanjiaping and Wuquanshan sections, the percentages of 300–200 and 2600–1600 Ma zircons increase from the lower to the upper part of the Wuquan Formation. Fig. 8 shows that this age population increases from 49% and 47% in samples Fanjiaping50m and Fanjiaping90m to 54% in sample Fanjiaping280m; similarly, it increases from 54% in sample Wuquanshan8m to 63% in sample Wuquanshan36m (Fig. 8D to B, G to F). One exception is sample

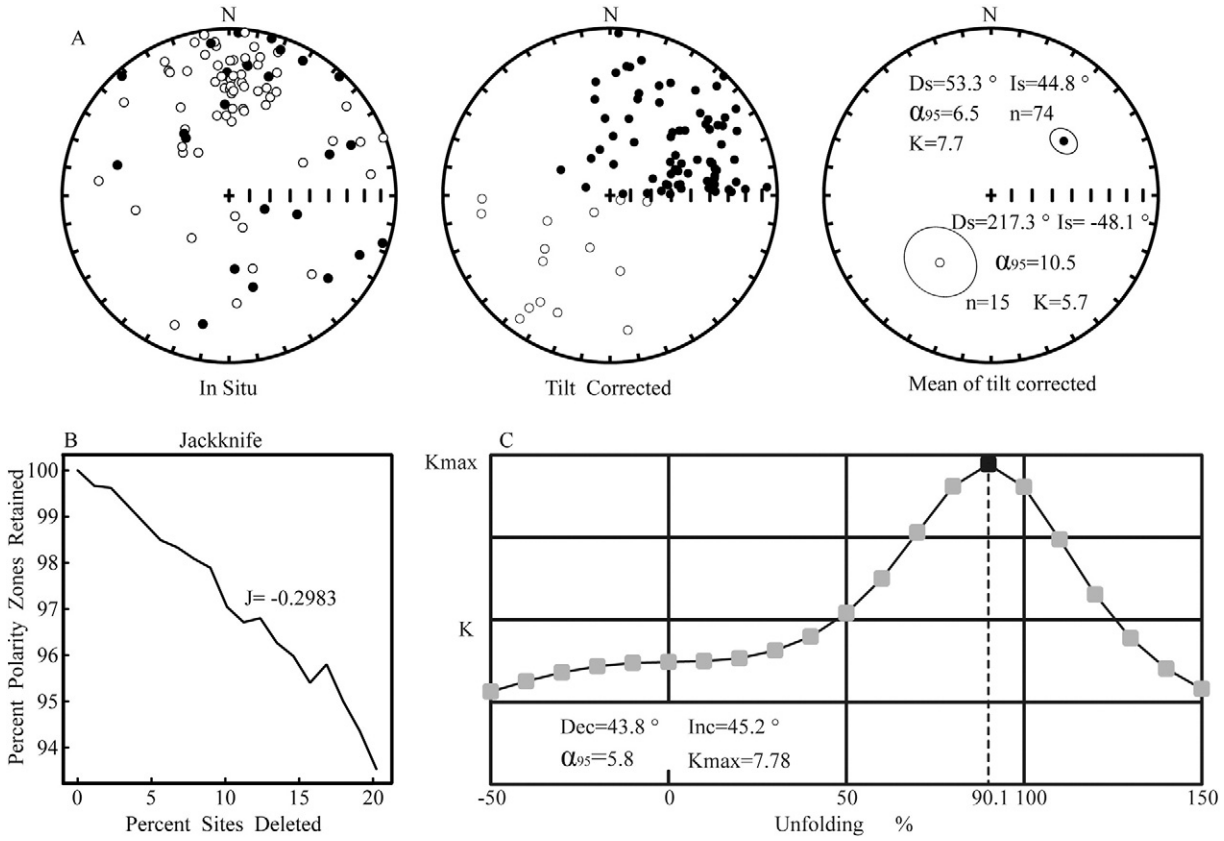

Fig. 6. Results of assessment of the reliability of the magnetostratigraphic results for the Fanjiaping section. (A) Equal-area projection of all 89 ChRM directions in in situ, tilt corrected, and mean of tilt corrected (with oval of 95% confidence) coordinates (Tauxe, 1998). Downward (upward) directions are shown as filled (open) circles. (B) Results of jackknife analysis, which indicates that the magnetostratigraphy has recovered >95% of the true number of polarity intervals (Tauxe and Gallet, 1991). (C) McFadden (1990) fold test for the obtained ChRMs, which indicate a maximum grouping at 90.1% unfolding and thus a positive fold test.

Wuquanshan70m, which exhibits distinct peaks from 500 to 400 Ma and from 1000 to 800 Ma (Fig. 8E), similar to the sample from the Leitan River draining the Maxian-Xinglong Mountains (Fig. 8K).

5. Discussion

5.1. Age of the Wuquan Formation

Previous studies have provided preliminary biostratigraphic and sequence-stratigraphic framework for the Wuquan Formation in the Lanzhou Basin. These findings are summarized below. A serious of fossils, e.g., *Coelodonta antiquitatis*, *Equus sanmeniensis*, and *Ochotona* sp., were discovered, from which we can infer that the strata were formed in the early Pleistocene (Gu and Zhang, 1987; Gansu BGMR, 1988). Early magnetostratigraphic dating of the 200-m thickness of loess overlying the Wuquanshan section indicated that the basal age of the loess was ~1.6 Ma (Li et al., 1999; Fig. 7), while a recent study of the 416-m-long Xijin loess drill core indicates that the age of the top of the Wuquan Formation is not later than 2.2 Ma (Zhang et al., 2016). As the Xijin drilling is located in the Qilihe subsidence area, and the Wuquanshan section is on the hanging wall of the Leitanhe thrust fault (Fig. 2), their difference in terms of basal loess age is probably owing to differential erosion processes. A magnetostratigraphic investigation of the red beds underlying the Wuquan Formation in the Nanshan section suggests that the age of the top of the stratum dates from 3.5 Ma (Sun et al., 2011). Although this result is in conflict with the early Miocene fossil records from the same section (Qiu and Gu, 1988), further paleomagnetic results are in accord with the fossil records and confirm that the deposition of the Xianshuihe Formation ended in the latest Miocene (Y.B. Zhang et al., 2014; Ao et al., 2016). Thus, the age of the Wuquan Formation is reliably constrained to span the interval from the Pliocene to the early Pleistocene.

The cosmogenic nuclide (^{10}Be and ^{26}Al) burial ages of the two samples from the Wuquanshan section are 2.72 + 0.54/−0.46 and 2.85 + 0.60/−0.52 Ma (Table 1 and Fig. 7), which are in accordance with the biostratigraphic and sequence-stratigraphic framework of the Wuquan Formation. Our magnetostratigraphic study of the Fanjiaping section yielded three normal polarity zones (N1-N3) and two reversed polarity zones (R1 and R2) (Fig. 7). Based on the cosmogenic nuclide burial ages and stratigraphic constraints, the three normal polarity zones (N1-N3) are correlated to C2An.1n (3.032–2.581 Ma), C2An.2n (3.207–3.116 Ma), and C2An.3n (3.596–3.330 Ma) of the GPTS; and the two reversed polarity zones (R1 and R2) are correlated with C2An.1r (Kaena event) and C2An.2r (Mammoth event) of the GPTS (Hilgen et al., 2012). Therefore, the age of the top of the Wuquan Formation should be ≥2.2 Ma, and the basal age should be ≤3.6 Ma. Furthermore, the evidence of plant pollen from the Fanjiaping section shows that the age of the Wuquan conglomerate is probably of late Pliocene age (Yuan, 2007), roughly equivalent to the Jishi conglomerate in the Linxia Basin (Fang et al., 2003). Thus, we propose that the age of the Wuquan Formation is reliably constrained to ~3.6–2.2 Ma.

5.2. Sedimentology and provenance of the Wuquan Formation

The Wuquan Formation is composed principally of imbricated, well-rounded, and well-sorted cobble conglomerates intercalated with pebble and sandstone layers with graded bedding, cross-bedding, and channelized structures (Fig. 3). From the depocenter to the basin edges, the thickness of the Wuquan Formation is 443 m in the Fanjiaping section, 272 m in the Xijincun (Xiaojiazhuang) drill core, and 100 m in the Wuquanshan section (Gansu BGMR, 1988; Wu et al.,

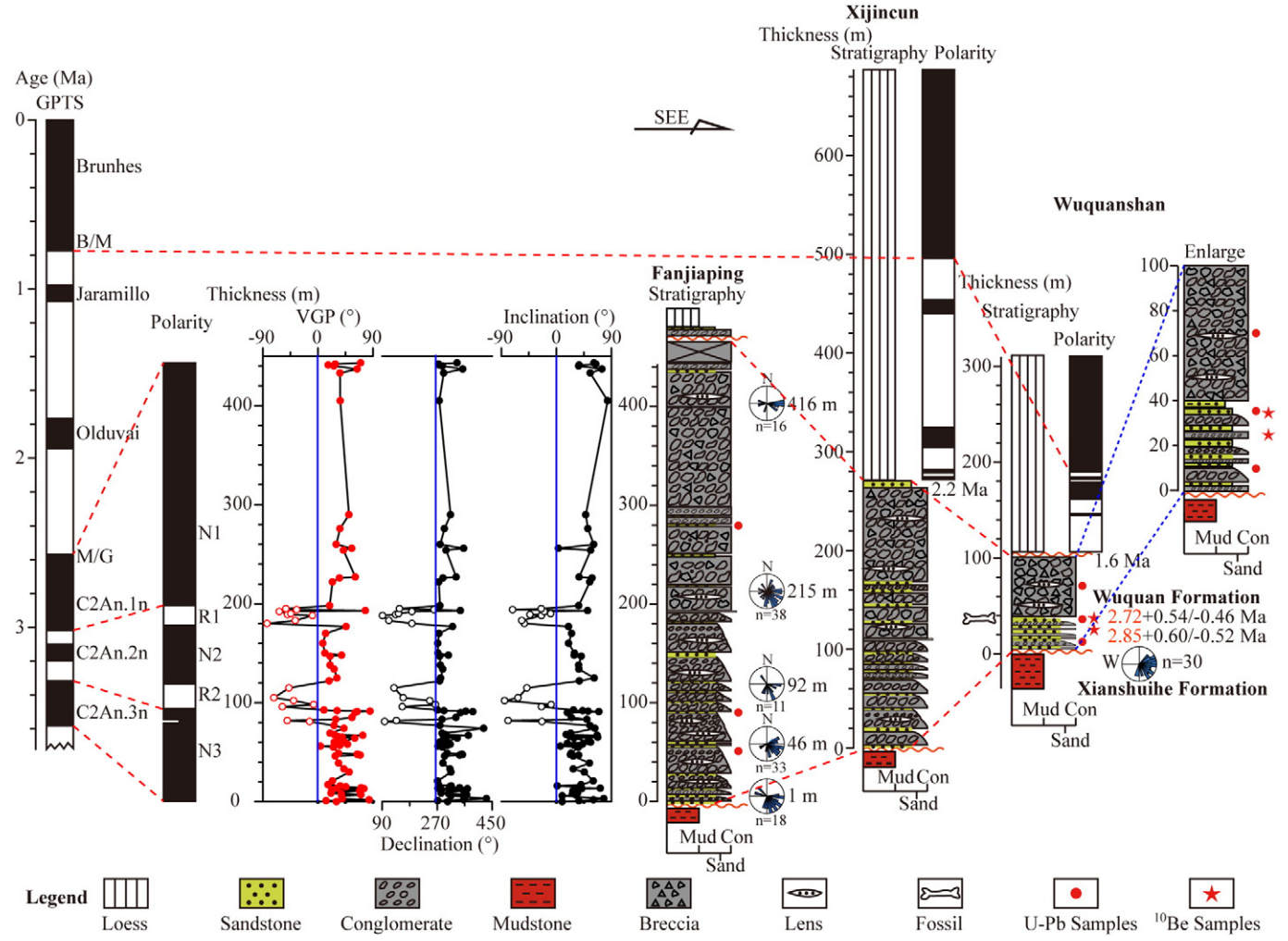

Fig. 7. Comparison of lithologic sequences, paleocurrent directions, and magnetostratigraphic results for the Fanjiaping section and of cosmogenic nuclide burial dating results of the Wuquanshan section with those from the Xijincun drill core in the Lanzhou Basin. Sedimentary facies based on field investigations are shown for comparison. VGP: virtual geomagnetic pole, GPTS: geomagnetic polarity time scale (Hilgen et al., 2012). The age of the Xijin loess is about 2.2 Ma (Zhang et al., 2016) and that of the Wuquanshan loess is about 1.6 Ma (Li et al., 1999). The Wuquan Formation record from the Xinjin drill core is modified from Gansu BGMR (1988); the fossils at the bottom of the upper part of the Wuquan Formation were from the Wuquanshan section (Gansu BGMR, 1988).

1988; Figs. 2 and 7). In addition, the grain size and gravel proportion decrease from the Fanjiaping section to the Wuquanshan section. These sedimentary characteristics associated with continuous accumulation of conglomerate beds indicate a stacked fluvial architecture (Bridgland and Westaway, 2014), consistent with previous studies (Gu and Zhang, 1987; Wu et al., 1988; Yuan, 2007; Nie et al., 2015). More importantly, the new quantitative evidence of grain size, conglomerate composition, and paleocurrent directions indicate that the Wuquan Formation resembles the Yellow River terraces (Fig. 3), which also suggests that the late Pliocene fluvial system was likely close to the drainage scale, flux capacity, and flow direction of the Quaternary Yellow River crossing the Lanzhou Basin.

It is generally accepted that the detrital zircons from the upper reaches of the modern Yellow River across the Songpan-Ganzi, East Kunlun, and West Qinling terranes are dominated by an age range of 300–200 Ma with additional broader ranges of 500–400, 1000–800, and 2600–1600 Ma (Stevens et al., 2013; Kong et al., 2014; Nie et al., 2015; Fig. 8I). These age ranges are closely tied to the widespread Triassic sediments and Permo-Triassic plutons in this region (Lease et al., 2007; Weislogel et al., 2010). In contrast, the detrital zircons from the Datong River and Huangshui River draining the Qilian and Laji mountains are characterized by a prominent age population between 500 and 400 Ma (Fig. 8J), in accord with previous studies of the dominant lower Paleozoic sedimentary rocks and plutons across these ranges (Gehrels et al., 2003; Lease et al., 2007; Tung et al., 2016). The detrital zircons from the Leitan River exhibit multiple age populations (Fig. 8K), among which the 500–400 and 1000–900 Ma zircons can be related to the lower Paleozoic plutons and Precambrian basement in the Maxian Mountains (Tung et al., 2016), while the remainder can perhaps be attributed to the Cretaceous and Cenozoic

Table 1
Cosmogenic nuclide burial ages for samples from the Wuquanshan section.

Sample	Latitude	Longitude	Depth	^{10}Be (10^3at/g)	^{26}Al (10^3at/g)	^{26}Al/^{10}Be ratio	Age (Ma)
WQA	36°1.865′	103°49.805′	32 m	9.23 ± 0.83	17.87 ± 3.68	1.94 ± 0.43	2.72 + 0.54/−0.46
WQB	36°1.943′	103°49.480′	25 m	8.47 ± 0.97	15.49 ± 3.47	1.83 ± 0.46	2.85 + 0.60/−0.52

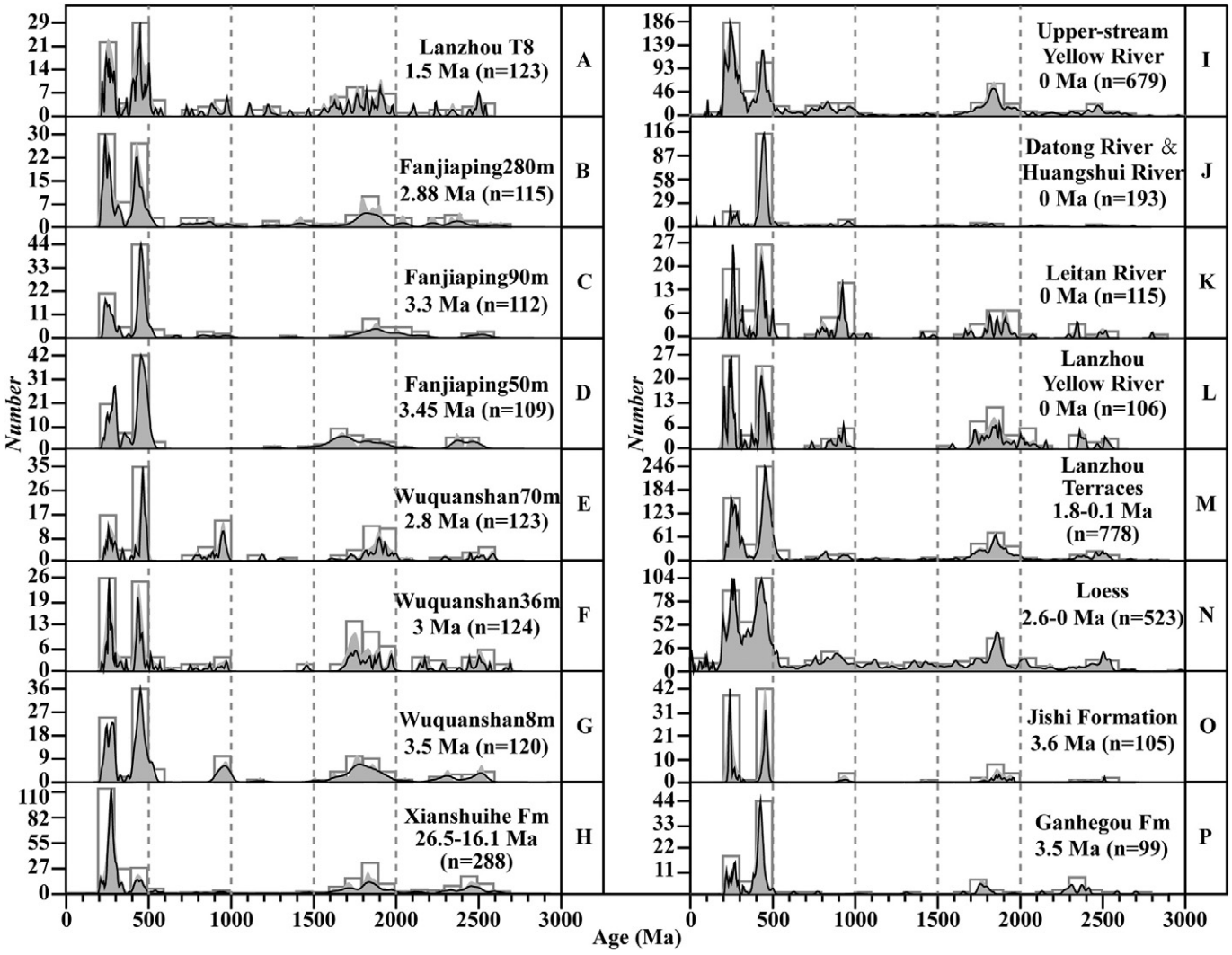

Fig. 8. Compilation of detrital zircon U—Pb age spectra. Black curves are probability density functions (PDF); grey shaded areas are kernel density estimates (KDE). Rectangles are histograms of age distributions. (A) New data from the eighth Yellow River terrace in the Lanzhou Basin. (B-G) New data for the Wuquan Formation from the Fanjiaping and Wuquanshan sections (sample locations are shown in Fig. 7). (H) Published data for the Xianshuihe Formation in the Lanzhou Basin (Wang et al., 2016). (I) Published data for the upper reaches of the Yellow River beyond the Laji Mountains (Nie et al., 2015, integrated from samples 1–6 in Fig. 1). (J) Integration of new data from the Datong River and published data from the Huangshui River, which both originate from the Qilian Mountains (Nie et al., 2015; samples 7 and 8 in Fig. 1). (K) New data for the Leitan River. (L) New data for the Yellow River in the Lanzhou Basin. (M) Integration of all published data for the terraces in the Lanzhou Basin (Nie et al., 2015). (N) Integration of all published data for loess (Pullen et al., 2011; Stevens et al., 2013). (O) Published data for the Jishi Formation in the Linxia Basin (Nie et al., 2015). (P) Published data for the Ganhegou Formation in the Tongxin Basin (Wang et al., 2013).

sedimentary covers. Given these characteristics of regional zircon age distribution, we infer that the 300–200 and 2600–1600 Ma zircons of the Wuquan Formation were mainly derived from the plateau areas upstream of the Lanzhou Basin; the 500–400 and 1000–900 Ma zircons may be in part derived from the adjacent Qilian, Laji, and Maxian mountains. Consequently, the late Pliocene river under discussion did not originate from any individual range, but rather it integrated the sediment supply of the numerous tributaries that drained the various tectonic zones of the northeastern TP during the late Pliocene. Furthermore, the similarity of the detrital zircon age spectra between the Wuquan Formation and the Yellow River terraces and bars in the Lanzhou Basin (Fig. 8B–G vs. A, I and M) also implies that the source zone of the Wuquan Formation was close to the drainage area of the upper reaches of the Yellow River. But considering that the zircon age spectra from the terraces and modern bars in the Lanzhou Basin are not distinctly different (Nie et al., 2015; Fig. 8L vs. M), in addition to which the Yellow River had not reached to the Anyemaqen Mountains prior to 0.1 Ma (Harkins et al., 2007), we suggest that the uppermost source region was restricted to the West Qinling Mountains.

5.3. Late Cenozoic drainage development

Given the above context, the fluvial system forming the Wuquan Formation was probably a large-scale drainage system originating from several tectonic zones of the northeastern TP, close to the Pleistocene Yellow River running across the Lanzhou Basin. Furthermore, two sequences of Pliocene conglomerate-sand fluvial strata have also been found in the Linxia Basin (upstream) and the Tongxin Basin (downstream), which were dated to start from ≤4–3.6 Ma ago (Fang et al., 2003; Wang et al., 2013), consistent with the basal age of the Wuquan Formation. The detrital zircon ages from these two strata (Wang et al., 2013; Nie et al., 2015) are comparable to those of the Wuquan Formation (Fig. 8B–G vs. O and P), implying that the Pliocene fluvial strata within these three basins should be correlated rather than isolated basin-filling sequences. Despite there being no Pliocene provenance data to track further downstream fluvial deposits, the outcrop strata and drilling records reveal that a large fluvial system connecting the Tongxin Basin existed in the Yinchuan-Hetao Basin as early as the late Pliocene (Xu et al., 2012; Liang et al., 2013; Wang et al., 2015; B.F. Li et al., 2017).

The detrital zircon age spectra of the Wuquan Formation also resemble those of Quaternary loess from the Loess Plateau (Fig. 8B–G vs. N), which has been explained in terms of the loess sediments being derived from the deposits of the Pliocene river, which transported them into the northern arid lands (Nie et al., 2015). Therefore, the various lines of evidence suggest that a broad drainage system flowing through the northeastern TP and discharging sediments into the northern lowlands, possibly approximated to the modern Yellow River catchment from the West Qinling and Qilian mountains to the Yinchuan-Hetao Basin, has been established by ~3.6 Ma.

This discovery of late Pliocene exorheic drainage from the northeastern TP calls for a change in understanding of the formation of the Yellow River terraces since ~1.8 Ma ago, which were thought to record the earliest draining of the northeastern TP upon its transition from endorheic basins (Li et al., 1997; Craddock et al., 2010). For instance, although the Linxia Basin is indeed occupied by lacustrine deposits underling the uppermost terrace (Li et al., 1996; Fang et al., 2003), as discussed above, the late Pliocene fluvial strata in the Linxia and Lanzhou basins should be correlated within the context of drainage flowing out of the northeastern TP. Thus, further insight into the sedimentary and geomorphic changes is required. Based on field measurements, we found that the dip angle of strata in the Fanjiaping section decreases upward 56° to 26°, showing their syntectonic development (Fig. 2). Subsequently, the strata of the Wuquan Formation in both sections were upthrust with high dip angles, resulting in a regional scale (>20 km) fold that is overprinted by a series of transtensional faults after deposition (Yuan, 2007; Yuan et al., 2008; Fig. 2). The accumulation of late Miocene-Pliocene growth strata and their subsequent deformation have also been observed in the Linxia Basin (Li et al., 1996, 2014). This indicates a progressive tectonism between the West Qinling and the Lanzhou basins from the late Miocene to the Pliocene, followed by an abrupt intensification of compression in the early Pleistocene. The river incision on a peneplain surface in the Xining Basin reflects a slow uplift rate during the late Miocene-Pliocene and accelerated uplift since ~2 Ma (Vandenberghe et al., 2011), synchronous with the regional tectonic change. The Maxian-Xinglong Mountains adjacent to these regions should also have experienced a similar stepwise growth and abrupt uplift in the early Pleistocene (J.J. Li et al., 2017). We suggest that the strong mountain uplift had the effect of damming and interrupting the paleo-drainage and was associated with the infilling of the Linxia Basin with lacustrine sediments during 2.2–1.8 Ma (Li et al., 1996; Fang et al., 2003). The formation of terraces in association with river incision since 1.8 Ma was thus a further development of external drainage on the basis of previous draining and tectonic-geomorphic evolution.

Conversely, the formation of the Yellow River has been estimated to start from the Eocene, based on tectonic regime and on ancient sediments distributed along the two pathways of the modern Yellow River and the Weihe River (Lin et al., 2001). However, later studies suggest that the large region from the West Qinling Fault to the Haiyuan Fault was a low-lying endorheic area from the Eocene to the Miocene, characterized by abundant gypsum, marlstones, and other lacustrine sediments within a series of subbasins (Yue et al., 2000; Fang et al., 2003, 2005; Wang et al., 2013, 2016; Liu et al., 2015). Moreover, the lithology, paleocurrent direction, and detrital zircon age spectra of the Wuquan Formation are significantly different to those of the underlying red beds in the Lanzhou Basin (Fig. 8B–G vs. H). The spatial difference of provenance of the Oligocene-Miocene sediments in the Lanzhou, Tianshui, and Tongxin basins can also be obtained by comparing their detrital zircon age spectra (Wang et al., 2013, 2016; Liu et al., 2015). This means that Eocene-Miocene drainage flowing out of the northeastern TP is unlikely unless some credible evidence can support this interpretation.

Based on the above considerations, we conclude that the remarkable transition from internal to external drainage in the northeastern TP probably occurred at ~3.6 Ma. Over the lower reach of the Yellow River, although it was suggested that the Jinshaan Gorge was initially incised between 3.7 and 1.2 Ma (Pan et al., 2011, 2012; Hu et al., 2016), the downstream incision of the Fenwei graben and Sanmen Gorge is thought to have started as late as 1.2 Ma ago (Kong et al., 2014; Hu et al., 2017). Furthermore, in the absence of sediment tracking in the middle and lower reaches, we are unable to estimate whether the late Pliocene drainage was internal to hinterland basins or connected to the ocean. But the important implication is that the endorheic to exorheic transition occurred more than once. Meanwhile, there is no doubt that the development of the Yellow River toward the modern through-going pattern was a dynamic process, integrating previous drainage systems, meanwhile balancing local and regional uplift, excavation, and deposition (Harkins et al., 2007; Pan et al., 2009; Perrineau et al., 2011; Vandenberghe et al., 2011; H.P. Zhang et al., 2014; Hu et al., 2017; B.F. Li et al., 2017).

5.4. Fluvial system response to tectonic deformation and climate change

There are three major factors (uplift, climate change, and eustasy) that control the formation of a river system and fluvial incision (Merritts et al., 1994; Schumm et al., 2000; Vandenberghe, 2003; Maddy et al., 2008; Westaway, 2009; Zheng et al., 2013; Bridgland and Westaway, 2014). The effect of eustasy on the upper reach of the Yellow River can be ignored as it lies ~3300 km upstream of the estuary; however, the effects of tectonic uplift and climate change on the formation and development of the river system have been debated (Li et al., 1996, 1997; Miao et al., 2008; Pan et al., 2009, 2011; Craddock et al., 2010; Vandenberghe et al., 2011; Wang et al., 2012; Kong et al., 2014; H.P. Zhang et al., 2014; Hu et al., 2016, 2017). The late Pliocene out-flowing drainage presented in this study holds new implications for understanding regional geomorphic evolution associated with tectonics and climate change.

Over the past decade, expanding tectonic and sedimentological studies have demonstrated that the growth of northeastern TP started from the Eocene, progressed through the Oligocene-middle Miocene, and accelerated in the late Miocene (Yuan et al., 2013; Craddock et al., 2014; Lease, 2014, and references therein). In particular, the Pliocene-Quaternary occurrence of widespread conglomerates, the huge rise of the accumulation rates, and intensified surface deformation and incision (within and around the northeastern TP) reflect expanded plateau growth and accelerated denudation (Meyer et al., 1998; Tapponnier et al., 2001; Pan et al., 2009, 2011; Vandenberghe et al., 2011; Li et al., 2014; J.J. Li et al., 2017). We speculate that the northeastern TP was elevated beyond a critical geomorphological threshold to result in drainage flowing out during the Pliocene. At the same time, the extension and sinking of the Yinchuan-Hetao graben in response to the enhanced left-lateral slippage of the Haiyuan Fault and eastward expansion of the northeastern TP probably opened a downstream path for paleo-drainage (Burchfiel et al., 1991; Lin et al., 2001; Lei et al., 2016). Thus, the uplift of the TP and its periphery and the subsidence of the distal region may have triggered a major reconfiguration of the regional river systems.

In addition to tectonic uplift, climate change is another important factor in triggering changes in river discharge and sediment supply, which controls channel aggradation, incision processes, and fluvial styles (Vandenberghe, 2003; Nanson et al., 2008). Previous studies have shown that northern hemisphere glaciation commenced in the late Miocene and intensified in the Pliocene, resulting in a global acceleration in erosion and sedimentation during ~4–2 Ma (Zachos et al., 2001; Zhang et al., 2001). In addition, the Asian summer monsoon also gradually intensified during ~4–3 Ma, resulting in increased precipitation and erosion in northern China (An et al., 2001; Zhang et al., 2009; Fu et al., 2013; Nie et al., 2014). The greatly increased precipitation associated with the strengthening of the summer monsoon would have provided the abundance of water to promote the development of an enormous fluvial system in the eastern TP. Therefore, we can

conclude that the significant climatic shift at about 3.6 Ma was a major factor responsible for the establishment of the paleo-drainage.

Consequently, in contrast to the subsequent Yellow River, the initial formation of the paleo-drainage represented by the Wuquan Formation at ~3.6 Ma is better in concordance with the dramatic uplift of the northeastern TP, an intensified Asian summer monsoon, and global increase in erosion rates from the late Pliocene onward (Meyer et al., 1998; An et al., 2001; Tapponnier et al., 2001; Zachos et al., 2001; Zhang et al., 2001; Zhang et al., 2009; Li et al., 2014; Nie et al., 2014). More importantly, the late Pliocene fluvial sequence reveals more than one transition of regional drainage in endorheic and exorheic patterns — this fluctuation perhaps linked to tectonic and/or climatic change. Thus, the development from the late Pliocene drainage to the Yellow River reflects the interactions between landscape evolution, tectonic deformation, and climate change.

6. Conclusion

The Wuquan Formation, which is well preserved in the Lanzhou Basin, is a major fluvial archive of information about the establishment and evolution of the paleo-drainage system in the northeastern TP. Our new magnetostratigraphy for the Fanjiaping section and cosmogenic nuclide burial dating results for the Wuquanshan section constrain the age of the Wuquan Formation to ~3.6–2.2 Ma. Detailed analyses of sedimentary structure, conglomerate composition, paleocurrent direction, and detrital zircon U—Pb age provenance provide significant insights into the origin of the Wuquan Formation and its relationship with the evolution of the Yellow River system. The results indicate that the exorheic drainage of the northeastern TP was established at ~3.6 Ma. The formation of the upper reaches of the modern Yellow River since 1.8 Ma was thus a further development of external drainage on the basis of previous draining and tectonic-geomorphic evolution. Consequently, the endorheic to exorheic transition of drainage in the northeastern TP occurred more than once, synchronous with the uplift of the northeastern TP and the major climatic transition.

Acknowledgements

We are grateful to Xiuxi Wang, Zhengchuang Hui, Jia Liu, and Cheng Yang for assistance with field sampling and laboratory analyses. This paper has benefited from language correction, valuable comments, and constructive suggestions by Professor David Bridgland, Jef Vandenberghe, Jan Bloemendal, and two other anonymous reviewers, whose efforts are gratefully acknowledged. We would like to express our sincere gratitude to Editor Richard A. Marston for his hard work on this manuscript. This research was supported by the National Natural Science Foundation of China (grant no. 41330745), the (973) National Basic Research Program of China (grant no. 2013CB956403), the National Natural Science Foundation of China (grant nos. 41101012 and 41301216), and the Fundamental Research Funds for the Central Universities (lzujbky-2015-223).

References

An, Z.S., Kutzbach, J.E., Prell, W.L., Porter, S.C., 2001. Evolution of Asian monsoons and phased uplift of the Himalaya-Tibetan plateau since Late Miocene times. Nature 411, 62–66.

Ao, H., Roberts, A.P., Dekkers, M.J., Liu, X.D., Rohling, E.J., Shi, Z.G., An, Z.S., Zhao, X., 2016. Late Miocene-Pliocene Asian monsoon intensification linked to Antarctic ice-sheet growth. Earth Planet. Sci. Lett. 444, 75–87.

Bridgland, D., Westaway, R., 2014. Quaternary fluvial archives and landscape evolution: a global synthesis. Proc. Geol. Assoc. 125, 600–629.

Burbank, D.W., Li, J.J., 1985. Age and palaeoclimatic significance of the loess of Lanzhou, north China. Nature 316, 429–431.

Burchfiel, B.C., Zhang, P.Z., Wang, Y.P., Zhang, W.Q., Song, F.M., Deng, Q.D., Molnar, P., Royden, L., 1991. Geology of the Haiyuan fault zone, Ningxia-Hui autonomous region, China, and its relation to the evolution of the northeastern margin of the Tibetan plateau. Tectonics 10, 1091–1110.

Clark, M.K., Schoenbohm, L.M., Royden, L.H., Whipple, K.X., Burchfiel, B.C., Zhang, X., Tang, W., Wang, E., Chen, L., 2004. Surface uplift, tectonics, and erosion of eastern Tibet from large-scale drainage patterns. Tectonics 23, TC1006. https://doi.org/10.1029/2002TC001402.

Clift, P.D., Blusztajn, J., 2005. Reorganization of the western Himalayan river system after five million years ago. Nature 438, 1001–1003.

Craddock, W.H., Kirby, E., Harkins, W.N., Zhang, H.P., Shi, X.H., Liu, J.H., 2010. Rapid fluvial incision along the Yellow River during headward basin integration. Nat. Geosci. 3, 209–213.

Craddock, W.H., Kirby, E., Zhang, H.P., Clark, M.K., Champagnac, J.D., Yuan, D.Y., 2014. Rates and style of Cenozoic deformation around the Gonghe Basin, northeastern Tibetan plateau. Geosphere 10, 1255–1282.

DeGraaff-Surpless, K., Mahoney, J.B., Wooden, J.L., McWilliams, M.O., 2003. Lithofacies control in detrital zircon provenance studies: insights from the cretaceous Methow basin, southern Canadian cordillera. Geol. Soc. Am. Bull. 115, 899–915.

Deng, C.L., Zhu, R., Jackson, M.J., Verosub, K.L., Singer, M.J., 2001. Variability of the temperature-dependent susceptibility of the Holocene Eolian deposits in the Chinese Loess Plateau: a pedogenesis indicator. Phys. Chem. Earth Solid Earth Geod. 26, 873–878.

Deng, C.L., Vidic, N.J., Verosub, K.L., Singer, M.J., Liu, Q.S., Shaw, J., Zhu, R.X., 2005. Mineral magnetic variation of the Jiaodao Chinese loess/paleosol sequence and its bearing on long-term climatic variability. J. Geophys. Res. 110, B03103. https://doi.org/10.1029/2004JB003451.

Deng, C.L., Shaw, J., Liu, Q.S., Pan, Y.X., Zhu, R.X., 2006. Mineral magnetic variation of the Jingbian loess/paleosol sequence in the northern Loess Plateau of China: implications for quaternary development of Asian aridification and cooling. Earth Planet. Sci. Lett. 241, 248–259.

Evans, M.E., Heller, F., 2003. Environmental Magnetism: Principles and Applications of Enviromagnetics. Academic Press, New York.

Fang, X.M., Garzione, C., Van der Voo, R., Li, J.J., Fan, M.J., 2003. Flexural subsidence by 29 Ma on the NE edge of Tibet from the magnetostratigraphy of Linxia Basin, China. Earth Planet. Sci. Lett. 210, 545–560.

Fang, X.M., Yan, M.D., Van der Voo, R., Rea, D.K., Song, C.H., Parés, J.M., Gao, J.P., Nie, J.S., Dai, S., 2005. Late Cenozoic deformation and uplift of the NE Tibetan Plateau: evidence from high-resolution magnetostratigraphy of the Guide Basin, Qinghai Province, China. Geol. Soc. Am. Bull. 117, 1208–1225.

Fu, C.F., An, Z.S., Qiang, X.K., Bloemendal, J., Song, Y.G., Chang, H., 2013. Magnetostratigraphic determination of the age of ancient Lake Qinghai, and record of the east Asian monsoon since 4.63 Ma. Geology 41, 875–878.

Gansu BGMR (Gansu Bureau of Geology and Mineral Resource), 1988. Report of Quaternary Geology of Lanzhou (1:50,000). Hydrogeological Team Publishing House, Lanzhou (in Chinese).

Gehrels, G.E., Yin, A., Wang, X.F., 2003. Detrital-zircon geochronology of the northeastern Tibetan plateau. Geol. Soc. Am. Bull. 115, 881–896.

Granger, D.E., Muzikar, P.F., 2001. Dating sediment burial with in situ-produced cosmogenic nuclides theory, techniques, and limitations. Earth Planet. Sci. Lett. 188, 269–281.

Gu, Z.G., Zhang, S.Y., 1987. Evidence of mammalian fossils in Wuquan conglomerate of early Pleistocene at Lanzhou and its neighborhood. J. Lanzhou Univ. (Nat. Sci.) 23, 114–121 (in Chinese, with English abstract).

Harkins, N., Kirby, E., Heimsath, A., Robinson, R., Reiser, U., 2007. Transient fluvial incision in the headwaters of the Yellow River, northeastern Tibet, China. J. Geophys. Res. 112: F03S04. https://doi.org/10.1029/2006JF000570.

Hilgen, F., Lourens, L., Van Dam, J., 2012. The Neogene period. In: Gradstein, F.M., Ogg, J.G., Schmitz, M.D., Ogg, G.M. (Eds.), The Geologic Time Scale. Elsevier, Amsterdam, pp. 923–978.

Hu, X.F., Kirby, E., Pan, B.T., Granger, D.E., Su, H., 2011. Cosmogenic burial ages reveal sediment reservoir dynamics along the Yellow River, China. Geology 39, 839–842.

Hu, Z.B., Pan, B.T., Guo, L.Y., Vandenberghe, J., Liu, X.P., Wang, J.P., Fan, Y.L., Mao, J.W., Gao, H.S., 2016. Rapid fluvial incision and headward erosion by the Yellow River along the Jinshaan gorge during the past 1.2 Ma as a result of tectonic extension. Quat. Sci. Rev. 133, 1–14.

Hu, Z.B., Pan, B.T., Bridgland, D., Vandenberghe, J., Guo, L.Y., Fan, Y.L., Westaway, R., 2017. The linking of the upper-middle and lower reaches of the Yellow River as a result of fluvial entrenchment. Quat. Sci. Rev. 166, 324–338.

Kirschvink, J.L., 1980. The least-squares method line and plane and the analysis of palaeomagnetic data. Geophys. J. Int. 62, 699–718.

Kong, P., Jia, J., Zheng, Y., 2014. Time constraints for the Yellow River traversing the Sanmen Gorge. Geochem. Geophys. Geosyst. 15, 395–407.

Lease, R.O., 2014. Cenozoic mountain building on the northeastern Tibetan Plateau. Geol. Soc. Am. Spec. Pap. 507, 115–127.

Lease, R.O., Burbank, D.W., Gehrels, G.E., Wang, Z.C., Yuan, D.Y., 2007. Signatures of mountain building: detrital zircon U/Pb ages from northeastern Tibet. Geology 35, 239–242.

Lei, Q.Y., Zhang, P.Z., Zheng, W.J., Chai, C.Z., Wang, W.T., Du, P., Yu, J.X., 2016. Dextral strike-slip of Sanguankou-Niushoushan fault zone and extension of arc tectonic belt in the northeastern margin of the Tibet Plateau. Sci. China Earth Sci. 59, 1025–1040.

Li, J.J., Fang, X.M., Ma, H.Z., Zhu, J.J., Pan, B.T., Chen, F.H., 1996. Geomorphological and environmental evolution in the upper reaches of the Yellow River during the late Cenozoic. Sci. China Ser. D Earth Sci. 39, 380–390.

Li, J.J., Fang, X.M., Van der Voo, R., Zhu, J.J., Niocaill, C.M., Ono, Y., Pan, B.T., Zhong, W., Wang, J.L., Sasaki, T., Zhang, Y.T., Cao, J.X., Kang, S.C., Wang, J.M., 1997. Magnetostratigraphic dating of river terraces: rapid and intermittent incision by the Yellow River of the northeastern margin of the Tibetan Plateau during the Quaternary. J. Geophys. Res. 1021, 10121–10132.

Li, J.J., Zhang, B., Zhu, J.J., Zhao, Z.J., Cao, J.X., 1999. Magneto-and pedo-stratigraphy of paleosol-loess sequences in the Lanzhou Basin: evidence for evolution of Huang He. Chin. Sci. Bull. 44, 119–128 (Supp.).

Li, J.J., Fang, X.M., Song, C.H., Pan, B.T., Ma, Y.Z., Yan, M.D., 2014. Late Miocene-quaternary rapid stepwise uplift of the NE Tibetan Plateau. Quat. Res. 81, 393–544.
Li, B.F., Sun, D.H., Xu, W.H., Wang, F., Liang, B.Q., Ma, Z.W., Wang, X., Li, Z.J., Chen, F.H., 2017. Paleomagnetic chronology and paleoenvironmental records from drill cores from the Hetao Basin and their implications for the formation of the Hobq Desert and the Yellow River. Quat. Sci. Rev. 156, 69–89.
Li, J.J., Ma, Z.H., Li, X.M., Peng, T.J., Guo, B.H., Zhang, J., Song, C.H., Liu, J., Hui, Z.C., Yu, H., Ye, X.Y., Liu, S.P., Wang, X.X., 2017. Late Miocene-Pliocene geomorphological evolution of the Xiaoshuizi Peneplain in the Maxian Mountains and its tectonic significance for the northeastern Tibetan Plateau. Geomorphology 295, 393–405.
Liang, H., Zhang, K., Fu, J.L., Li, S.B., Chen, J., Lu, K., 2013. The neotectonics in the Niushou Mountains, the northeastern margin of the Tibetan Plateau, China and its impact on the evolution of the Yellow River. Geosci. Front. 20, 182–189 (in Chinese, with English abstract).
Lin, A.M., Yang, Z.Y., Sun, Z.M., Yang, T.S., 2001. How and when did the Yellow River develop its square bend? Geology 29, 951–954.
Liu, S.P., Li, J.J., Stockli, D.F., Song, C.H., Nie, J.S., Peng, T.J., Wang, X.X., He, K., Hui, Z.C., Zhang, J., 2015. Late tertiary reorganizations of deformation in northeastern Tibet constrained by stratigraphy and provenance data from eastern Longzhong Basin. J. Geophys. Res. Solid Earth 120, 5804–5821.
Maddy, D., Demir, T., Bridgland, D.R., Veldkamp, A., Stemerdink, C., van der Schriek, T., Westaway, R., 2008. The early Pleistocene development of the Gediz River, western Turkey: an uplift-driven, climate-controlled system? Quat. Int. 189, 115–128.
McFadden, P.L., 1990. A new fold test for paleomagnetic studies. Geophys. J. Int. 103, 163–169.
Merritts, D.J., Vincent, K.R., Wohl, E.E., 1994. Long river profiles, tectonism, and eustasy: a guide to interpreting fluvial terraces. J. Geophys. Res. 99, 14031–14050.
Meyer, B., Tapponnier, P., Bourjot, L., Metivier, F., Gaudemer, Y., Peltzer, G., Guo, S.M., Chen, Z.T., 1998. Crustal thickening in Gansu-Qinghai, lithospheric mantle subduction, and oblique, strike-slip controlled growth of the Tibet Plateau. Geophys. J. Int. 135, 1–47.
Miao, X.D., Lu, H.Y., Li, Z., Cao, G.C., 2008. Paleocurrent and fabric analyses of the imbricated fluvial gravel deposits in Huangshui valley, the northeastern Tibetan Plateau, China. Geomorphology 99, 433–442.
Molnar, P., England, P.C., 1990. Late Cenozoic uplift of mountain ranges and global climate change; chicken or egg? Nature 346, 29–34.
Nanson, G.C., Price, D.M., Jones, B.G., Maroulis, J.C., Coleman, M., Bowman, H., Cohen, T.J., Pietsch, T.J., Larsen, J.R., 2008. Alluvial evidence for major climate and flow regime changes during the middle and late quaternary in eastern central Australia. Geomorphology 101, 109–129.
Nie, J.S., Stevens, T., Song, Y.G., King, J.W., Zhang, R., Ji, S.C., Gong, L.S., Cares, D., 2014. Pacific freshening drives Pliocene cooling and Asian monsoon intensification. Sci. Rep. 4, 5474. https://doi.org/10.1038/srep05474.
Nie, J.S., Stevens, T., Rittner, M., Stockli, D., Garzanti, E., Limonta, M., Bird, A., Ando, S., Vermeesch, P., Saylor, J., Lu, H.Y., Breecker, D., Hu, X.F., Liu, S.P., Resentini, A., Vezzoli, G., Peng, W.B., Carter, A., Ji, S.C., Pan, B.T., 2015. Loess Plateau storage of northeastern Tibetan Plateau-derived Yellow River sediment. Nat. Commun. 6, 1–8.
Nie, J.S., Garzione, C., Su, Q.D., Liu, Q.S., Zhang, R., Heslop, D., Necula, C., Zhang, S.H., Song, Y.G., Luo, Z., 2017. Dominant 100,000-year precipitation cyclicity in a late Miocene lake from northeast Tibet. Sci. Adv. 3, e1600762.
Nishiizumi, K., Imamura, M., Caffee, M.W., Southon, J.R., Finkel, R.C., McAninch, J., 2007. Absolute calibration of ^{10}Be AMS standards. Nucl. Instrum. Methods Phys. Res., Sect. B 258, 403–413.
Pan, B.T., Li, J.J., Cao, J.X., Chen, F.H., 1996. Study on the geomorphic evolution and development of the Yellow River in the Hualong Basin. J. Mt. Sci. 14, 153–158 (in Chinese, with English abstract).
Pan, B.T., Su, H., Hu, Z.B., Hu, X.F., Gao, H.S., Li, J.J., Kirby, E., 2009. Evaluating the role of climate and tectonics during non-steady incision of the Yellow River: evidence from a 1.24 Ma terrace record near Lanzhou, China. Quat. Sci. Rev. 28, 3281–3290.
Pan, B.T., Hu, Z.B., Wang, J.P., Vandenberghe, J., Hu, X.F., 2011. A magnetostratigraphic record of landscape development in the eastern Ordos Plateau, China: transition from Late Miocene and Early Pliocene stacked sedimentation to Late Pliocene and Quaternary uplift and incision by the Yellow River. Geomorphology 125, 225–238.
Pan, B.T., Hu, Z.B., Wang, J.P., Vandenberghe, J., Hu, X.F., Wen, Y.H., Li, Q.Y., Cao, B., 2012. The approximate age of the planation surface and the incision of the Yellow River. Palaeogeogr. Palaeoclimatol. Palaeoecol. 356-357, 54–61.
Perrineau, A., van der Woerd, J., Gaudemer, Y., Jing, Z., Pik, R., Papponnier, P., Thuizat, R., Zheng, R., 2011. Incision rate of the Yellow River in Northeastern Tibet constrained by ^{10}Be and ^{26}Al cosmogenic isotope dating of fluvial terraces: implications for catchment evolution and plateau building. J. Geol. Soc. Lond. 353, 189–219.
Pullen, A., Kapp, P., McCallister, A.T., Chang, H., Gehrels, G.E., Garzione, C.N., Heermance, R.V., Ding, L., 2011. Qaidam Basin and northern Tibetan Plateau as dust sources for the Chinese Loess Plateau and paleoclimatic implications. Geology 39, 1031–1034.
Qiu, Z.X., Gu, Z.G., 1988. A new locality yielding mid-tertiary mammals near Lanzhou, Gansu. Vertebr. Palasia. 26, 198–213 (in Chinese with English abstract).
Raymo, M.E., Ruddiman, W.F., 1992. Tectonic forcing of the late Cenozoic climate. Nature 359, 117–122.
Schumm, S.A., Dumont, J.F., Holbrook, J.M., 2000. Active Tectonics and Alluvial Rivers. Cambridge University Press, Cambridge, U. K.
Stevens, T., Carter, A., Watson, T.P., Vermeesch, P., Andò, S., Bird, A.F., Lu, H.Y., Garzanti, E., Cottam, M.A., Sevastjanova, I., 2013. Genetic linkage between the Yellow River, the Mu Us desert, and the Chinese Loess Plateau. Quat. Sci. Rev. 78, 355–368.
Sun, D.H., Zhang, Y.B., Han, F., Zhang, Y., Yi, Z.Y., Li, Z.J., Wang, F., Wu, S., Li, B.F., 2011. Magnetostratigraphy and palaeoenvironmental records for a Late Cenozoic sedimentary sequence from Lanzhou, Northeastern margin of the Tibetan Plateau. Glob. Planet. Chang. 76, 106–116.
Tapponnier, P., Xu, Z.Q., Roger, F., Meyer, B., Arnaud, N., Wittlinger, G., Yang, J.S., 2001. Oblique stepwise rise and growth of the Tibet Plateau. Science 294, 1671–1677.
Tauxe, L., 1998. Paleomagnetic Principles and Practice. Kluwer Academic Publishers, Dordrecht, pp. 121–170.
Tauxe, L., Gallet, Y., 1991. A jackknife for magnetostratigraphy. Geophys. Res. Lett. 18, 1783–1786.
Tung, K.A., Yang, H.Y., Yang, H.J., Smith, A., Liu, D.Y., Zhang, J.X., Wu, C.L., Shau, Y.H., Wen, D.J., Tseng, C.Y., 2016. Magma sources and petrogenesis of the early-middle Paleozoic backarc granitoids from the central part of the Qilian block, NW China. Gondwana Res. 38, 197–219.
Vandenberghe, J., 2003. Climate forcing of fluvial system development: an evolution of ideas. Quat. Sci. Rev. 22, 2053–2060.
Vandenberghe, J., Wang, X.Y., Lu, H.Y., 2011. The impact of differential tectonic movement on fluvial morphology and sedimentology along the northeastern Tibetan Plateau. Geomorphology 134, 171–185.
Vermeesch, P., 2012. On the visualisation of detrital age distributions. Chem. Geol. 312, 190–194.
Wang, X.Y., Lu, H.Y., Vandenberghe, J., Zheng, S., Van Balen, R.T., 2012. Late Miocene uplift of the NE Tibetan Plateau inferred from basin filling, planation and fluvial terraces in the Huang Shui catchment. Glob. Planet. Chang. 88-89, 10–19.
Wang, W.T., Zhang, P.Z., Zheng, D.W., Zhang, G.L., Zhang, H.P., Zheng, W.J., Chai, C.C., Kirby, E., 2013. Tertiary basin evolution along the northeastern margin of the Tibetan Plateau: evidence for basin formation during Oligocene transtension. Geol. Soc. Am. Bull. 125, 377–400.
Wang, P., Scherler, D., Liu-Zeng, J., Mey, J., Avouac, J., Zhang, Y.D., Shi, D.G., 2014. Tectonic control of Yarlung Tsangpo Gorge revealed by a buried canyon in southern Tibet. Science 346, 978–981.
Wang, J.P., Shen, M.M., Hu, J.M., Wei, M.J., Zhao, X.H., Liu, S.C., Li, X.L., Li, X.L., 2015. Magnetostratigraphy and its paleoclimatic significance of the PL02 borehole in the Yinchuan Basin. J. Asian Earth Sci. 114, 258–265.
Wang, W.T., Zhang, P.Z., Liu, C.C., Zheng, D.W., Yu, J.X., Zheng, W.J., Wang, Y.Z., Zhang, H.P., Chen, X.Y., 2016. Pulsed growth of the West Qinling at ~30 Ma in northeastern Tibet: evidence from Lanzhou Basin magnetostratigraphy and provenance. J. Geophys. Res. Solid Earth 121. https://doi.org/10.1002/2016JB013279.
Weislogel, A.L., Graham, S.A., Chang, E.Z., Wooden, J.L., Gehrels, G.E., 2010. Detrital zircon provenance from three turbidite depocenters of the middle-upper Triassic Songpan-Ganzi complex, central China: record of collisional tectonics, erosional exhumation, and sediment production. Geol. Soc. Am. Bull. 122, 2041–2062.
Westaway, R., 2009. Active crustal deformation beyond the SE margin of the Tibetan Plateau: constraints from the evolution of fluvial systems. Glob. Planet. Chang. 68, 395–417.
Whipple, K.X., 2009. The influence of climate on the tectonic evolution of mountain belts. Nat. Geosci. 2, 97–103.
Wu, A.B., Liu, J.K., Song, C.H., 1988. Approch on the characteristics of grain size and the origin of Wuquanshan Formation of lower Pleistocene series, Lanzhou Basin. J. Lanzhou Univ. (Nat. Sci.) 24, 108–118 (in Chinese, with English abstract).
Xu, W., Liu, Y., Zhao, J., Yan, J., Hao, Y., 2012. Geothermal Survey Report of Qixinghu Tourist Area in the Ordos, Inner Mongolia Autonomous Region (In Chinese).
Young, C.C., Bien, M.N., 1937. Cenozoic geology of the Kaolan-Yungteng area of central Kansu. Bull. Geol. Soc. China 16.
Yuan, D.Y., 2007. The Active Tectonic Framework and Deformation Features in Lanzhou Basin. Institute of Geology, Seismological Bureau of China (in Chinese, with English abstract).
Yuan, D.Y., Wang, L.M., He, W.G., Lu, B.C., Ge, W.P., Liu, X.W., Liang, M.J., Zheng, W.J., 2008. New progress of seismic active fault prospecting in Lanzhou city. Seismol. Geol. 30, 236–249 (in Chinese, with English abstract).
Yuan, D.Y., Ge, W.P., Chen, Z.W., Li, C.Y., Wang, Z.C., Zhang, H.P., Zhang, P.Z., Zheng, D.W., Zheng, W.J., Craddock, W.H., Dayem, K.E., Duvall, A.R., Hough, B.G., Lease, R.O., Champagnac, J.D., Burbank, D.W., Clark, M.K., Farley, K.A., Garzione, C.N., Kirby, E., Molnar, P., Roe, G.H., 2013. The growth of northeastern Tibet and its relevance to large-scale continental geodynamics: a review of recent studies. Tectonics 32, 1358–1370.
Yue, L.P., Heller, F., Qiu, Z.X., Zhang, L., Xie, G.P., Qiu, Z.D., Zhang, Y.X., 2000. Magnetostratigraphy and paleoenvironmental record of Tertiary deposits of Lanzhou Basin. Chin. Sci. Bull. 46, 770–774.
Zachos, J.C., Pagani, M., Sloan, L., Thomas, E., Billups, K., 2001. Trends, rhythms, and aberrations in global climate 65 Ma to present. Science 292, 686–693.
Zhai, Y.P., Cai, T.L., 1984. The tertiary system of Gansu province. Gansu Geol. 21, 1–40 (in Chinese).
Zhang, P.Z., Molnar, P., Downs, W.R., 2001. Increased sedimentation rates and grain sizes 2-4 Myr ago due to the influence of climate change on erosion rates. Nature 410, 891–897.
Zhang, Y.G., Ji, J., Balsam, W., Liu, L., Chen, J., 2009. Mid-Pliocene Asian monsoon intensification and the onset of northern hemisphere glaciation. Geology 37, 599–602.
Zhang, H.P., Zhang, P.Z., Champagnac, J.D., Molnar, P., Anderson, R.S., Kirby, E., Craddock, W.H., Liu, S.F., 2014. Pleistocene drainage reorganization driven by the isostatic response to deep incision into the northeastern Tibetan plateau. Geology 42, 303–306.
Zhang, Y.B., Sun, D.H., Li, Z.J., Wang, F., Wang, X., Li, B.F., Guo, F., Wu, S., 2014. Cenozoic record of aeolian sediment accumulation and aridification from Lanzhou, China, driven by Tibetan plateau uplift and global climate. Glob. Planet. Chang. 120, 1–15.
Zhang, J., Li, J.J., Guo, B.H., Ma, Z.H., Li, X.M., Ye, X.Y., Yu, H., Liu, J., Yang, C., Zhang, S.D., Song, C.H., Hui, Z.C., Peng, T.J., 2016. Magnetostratigraphic age and monsoonal evolution recorded by the thickest Quaternary loess deposit of the Lanzhou region, western Chinese Loess Plateau. Quat. Sci. Rev. 139, 17–29.
Zhao, Z.J., Granger, D.E., Chen, Y., Shu, Q., Liu, G.F., 2017. Cosmogenic nuclide burial dating of an alluvial conglomerate sequence: an example from the Hexi Corridor, NE Tibetan Plateau. Quat. Geochronol. 39, 68–78.
Zheng, H.B., Christopher, M.P., An, Z.S., Zhou, J., Dong, G.R., 2000. Pliocene uplift of the northern Tibetan Plateau. Geology 28, 715–718.
Zheng, H.B., Clift, P.D., Wang, P., Tada, R., Jia, J.T., He, M.Y., Jourdan, F., 2013. Pre-Miocene birth of the Yangtze River. Proc. Natl. Acad. Sci. 110, 7556–7561.